# Close Encounters between Periodic Light and Periodic Arrays of Quantum Emitters

Frieder Lindel,[1,2,3] Carlos J. Sánchez Martínez,[1,2] Johannes Feist,[1,2,*] and Francisco J. García-Vidal[1,2,†]
[1]Departamento de Física Teórica de la Materia Condensada, Universidad Autónoma de Madrid, E-28049 Madrid, Spain
[2]Condensed Matter Physics Center (IFIMAC), Universidad Autónoma de Madrid, E-28049 Madrid, Spain
[3]Institute for Theoretical Physics, ETH Zürich, CH-8093 Zürich, Switzerland

(Received 5 August 2025; revised 15 May 2026; accepted 21 July 2026; published 2 September 2026)

We introduce crystal polaritons, hybrid excitations formed when the collective excitations of a periodic quantum-emitter array strongly couple to the resonant Bloch modes of a metasurface. This realizes a cavity-QED platform in which periodic light and periodic matter are treated on the same footing, allowing strong collective light-matter coupling in an extended, lossy, and dispersive nanophotonic structure. To describe this regime, we develop a reciprocal-space few-mode quantization based on macroscopic quantum electrodynamics, which maps the metasurface resonances seen by the emitter array onto a cavity-QED Hamiltonian at each in-plane momentum. We show that both plasmonic surface-lattice resonances and dielectric bound states in the continuum can enter the strong-coupling regime with a single emitter per unit cell. As a consequence of the resonant nonlinearities of the resulting crystal polaritons, the platform enables quantum light generation with efficiencies orders of magnitude higher than those achieved in conventional nonlinear metasurfaces.

DOI: 10.1103/71nx-b83j

Confining photons in cavities can lead to strong coupling of single or few photonic modes to quantum emitters. This is at the heart of cavity quantum electrodynamics (QED), with applications in the generation of nonclassical states of light [1], quantum sensors [2], or in quantum information science [3]. However, traditional wavelength-sized cavities are restricted by the diffraction limit. While plasmonic nanoparticles overcome this via subwavelength confinement [4–6], they suffer from high losses that limit many quantum optical applications.

An alternative is provided by two-dimensional periodically structured surfaces (metasurfaces). Because their resonant modes extend over many unit cells, metasurfaces can combine subwavelength field confinement with mitigated losses [7]. They offer many exciting design possibilities to, e.g., support flat bands [8], topologically protected states [9,10], and lasing [11–13], or bound states in the continuum [14–17]. Consequently, they have become a well-established tool for manipulating classical [18,19] and quantum states of light [20,21], and have been used for strong light-matter coupling to dense molecular ensembles [22,23] leading to polariton lasing [24,25], polariton BECs [26], and polaritonic chemistry [27].

Arrays of quantum emitters in free space—such as cold atoms or molecules—have emerged as platforms for cooperative optics with applications in classical optics [28–30], nonlinear quantum optics [31–36], or quantum information processing [37,38] and quantum simulation [39].

Despite the versatility of these two periodic platforms, their combination has largely been restricted to the weak coupling regime [4,40], and previous *ab initio* frameworks that can accurately determine the quantized resonant modes of metasurfaces to which nearby emitters strongly couple are limited to the coupled-dipole approximation and linear response [41].

The regime we target here fundamentally differs from standard cavity QED and strong coupling of dense molecular ensembles to resonances supported by periodic nanostructures [22–27]. In a conventional cavity, a small number of *localized* photonic modes couple to localized matter excitations. By contrast, the relevant optical resonances in a metasurface are extended Bloch modes. As a difference also to dense ensembles of molecules, which behave essentially as classical harmonic oscillators, the discrete quantum emitters show much higher nonlinearities and therefore bear the potential to enter a nonlinear cavity QED regime. If a quantum-emitter array is made commensurable with the metasurface (see Fig. 1), this opens the possibility for coupling of collective spin-wave excitations of the emitter array with metasurface resonances at well defined Bloch momentum.

The central message of this Letter is that these two extended, periodic degrees of freedom—photonic and material—can hybridize strongly to form a new hybrid light-matter state that we term *crystal polaritons*. By identifying the coupled, lossy photonic modes of general metasurfaces via macroscopic QED, we obtain a cavity

*Contact author: johannes.feist@uam.es
†Contact author: fj.garcia@uam.es

 © 2026 American Physical Society

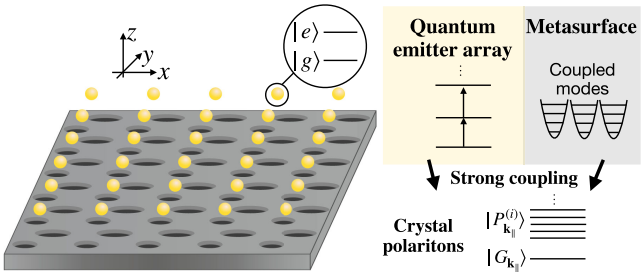


FIG. 1. Concept of a polaritonic quantum metasurface hosting crystal polaritons. A metasurface confines the light field in its vicinity that is strongly coupled to collective excitations of a quantum emitter array. Strong coupling of the quantized modes of the metasurface to the emitter array excitations leads to the formation of crystal polaritons.

QED-type Hamiltonian that gives full access to the quantum dynamics in the strong-coupling regime. We find that strong coupling is achievable with just a single emitter per unit cell, coupling to either bound states in the continuum of a dielectric array of nanoparticles or to surface lattice resonances (SLRs) of a metallic array of nanoparticles. This results in the hybridization of emitter spin waves and metasurface resonances into crystal polaritons. Furthermore, we show that laser driving of these crystal polaritons yields resonant quantum light generation with efficiencies many orders of magnitude higher than state-of-the-art nonlinear metasurfaces [42–45], reaching a strong nonlinear response with just one crystal polariton per 10.7 $\mu m^2$.

*Collective light-matter coupling in reciprocal space*—The essential simplification of the commensurable quantum metasurface (see Fig. 1) is that both subsystems share the same periodicity. The electromagnetic resonances of the metasurface are Bloch modes, and the collective excitations of the emitter array are spin waves carrying the same in-plane momentum. Strong coupling therefore does not occur between a localized emitter and a localized cavity mode, but between two extended Bloch-periodic degrees of freedom with the same Bloch momentum. The first task is to identify, for each in-plane momentum $\mathbf{k}_\parallel$ inside the Brillouin zone, which metasurface resonances are available to hybridize with the corresponding emitter-array excitation. As we show in the following, this information is contained in a reciprocal-space spectral density. It plays the same role as the local spectral density in ordinary cavity QED [46,47], but resolved in Bloch momentum and in the emitter positions within the unit cell. It determines the complex resonant frequencies of the electromagnetic environment seen by the spin wave and the strength with which this spin wave couples to them.

We characterize the emitters by their dipole operator $\hat{d}_i^{(h)} = d_i(\hat{\sigma}_i^{(h)} + \hat{\sigma}_i^{(h)\dagger})$ and orientation $\mathbf{n}^{(h)}$, as well as their position $\mathbf{r}_i^{(h)} = \mathbf{r}_0^{(h)} + \mathbf{R}_i$, with $\mathbf{r}_0^{(h)}$ denoting the position of the $h$ th dipole in the reference unit cell and $\{\mathbf{R}_i\}$ being the set of lattice vectors connecting the different unit cells. As we derive in detail in Supplemental Material (SM) [48], the Bloch-periodic spin-wave excitations of such emitter arrays $\hat{d}_{\mathbf{k}_\parallel}^{(h)} = \sum_i \hat{d}_i^{(h)} e^{-i\mathbf{k}_\parallel \cdot \mathbf{r}_i^{(h)}}$ couple to the continuum of field modes via the reciprocal-space spectral density of the metasurface

$$J_{h,h'}(\mathbf{k}_\parallel, \omega) = \frac{\mu_0 \omega^2}{\pi \hbar} d_h d_{h'} e^{-i\mathbf{k}_\parallel (r_0^{(h)} - r_0^{(h')})} \times \mathbf{n}^{(h)} \cdot \mathcal{G}_{\mathrm{AH}}\left(\mathbf{k}_\parallel, \mathbf{r}_0^{(h)}, \mathbf{r}_0^{(h')}, \omega\right) \cdot \mathbf{n}^{(h')}. \quad (1)$$

Here, $\mathcal{G}_{\mathrm{AH}}$ is the anti-Hermitian part of the Bloch-periodic Green tensor $\mathcal{G}(\mathbf{k}_\parallel, \mathbf{r}, \mathbf{r}', \omega) = \sum_i e^{i\mathbf{k}_\parallel \cdot \mathbf{R}_i} \mathbf{G}(\mathbf{r}, \mathbf{r}' + \mathbf{R}_i, \omega)$ [57,58] and dispersion and absorption was accounted for via macroscopic quantum electrodynamics [59].

We have thus identified $J_{h,h'}(\mathbf{k}_\parallel, \omega)$ as the key quantity that fully determines the optical environment of the metasurface seen by the emitter array and thus characterizes the extended resonances of metasurfaces. To illustrate this quantity, we consider a square array of silver nanospheres with radius $R = 50$ nm and lattice constant $a = 600$ nm that is coupled to an array of two-level emitters with a single emitter per unit cell located at different positions within the unit cell. The dipole moment of the two-level emitters is given by $d = 10$ D and the response of the silver spheres is described by a Drude permittivity as in Refs. [60,61].

As shown in Fig. 2, the maxima of the reciprocal-space spectral density $J \equiv J_{1,1}(\mathbf{k}_\parallel, \omega)$ follow the usual dispersion of the surface lattice resonances of the plasmonic array, resulting from the coupling of diffractive orders (Rayleigh anomalies) with the plasmonic resonance of the nanoparticles (here at 3.5 eV) [62]. Nevertheless, $J$ differs qualitatively from far-field observables such as reflectance, transmittance, or extinction of the array, see Fig. 2(c). In contrast to these quantities, $J$ depends on where the emitter sits inside the unit cell and on its dipole orientation, because it describes the collective near-field optical environment experienced by the matter excitation rather than the response of the bare metasurface to an external probe [see Fig. 2(b)].

*From the spectral density to a cavity-QED Hamiltonian*—The reciprocal-space spectral density identifies the optical resonances that the emitter-array spin waves can see, which we now map to a set of coupled lossy modes with spectral density identical to the *ab initio* result via a recently developed few-mode quantization scheme [63–68]. This step maps our setup to a typical cavity-QED Hamiltonian, with photonic Bloch modes and material spin waves appearing in equal terms.

The resulting few-mode Hamiltonian reads ($\hbar = 1$):

$$\hat{H}_{\mathbf{k}_\parallel} = \hat{H}_{e,\mathbf{k}_\parallel} + \sum_{i,j} \omega_{\mathbf{k}_\parallel,ij} \hat{a}_{\mathbf{k}_\parallel,i}^\dagger \hat{a}_{\mathbf{k}_\parallel,j} + \sum_{i,h} \left( g_{\mathbf{k}_\parallel,ih} \hat{d}_{\mathbf{k}_\parallel}^{(h)\dagger} \hat{a}_{\mathbf{k}_\parallel,i} + \mathrm{H.c.} \right). \quad (2)$$

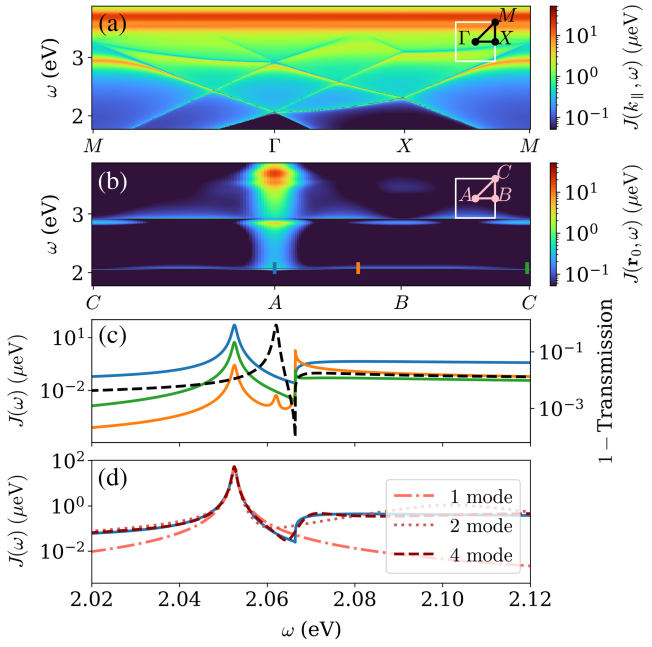


FIG. 2. Optical environment seen by a collective emitter array close to a square array of silver nanospheres. (a) Reciprocal space spectral density $J$ as a function of frequency and in-plane wave vector along a path in reciprocal space as indicated by the inset for an emitter array positioned in the center of the unit cell [$\mathbf{r}_\parallel = (0,0)$] and 10 nm above the nanospheres with dipole moment $d = 10$ D and orientation $\mathbf{n} = \mathbf{e}_z$. (b) $J$ at the Γ point ($\mathbf{k}_\parallel = \mathbf{0}$) for different emitter positions indicated by the colored rectangles in (b) [$\mathbf{r}_\parallel = (0,0)$, $\mathbf{r}_\parallel = (200,0)$ nm, $\mathbf{r}_\parallel = (300,300)$ nm]. (c) Cut through $J$ in (b) at three different positions indicated by vertical lines in (b) (colored lines) and the transmission through the array (black dashed line). (d) $J$ for an emitter at $A$ and the Γ point shown in (c) together with the fitted model spectral density $J_{\mathrm{mod}}$ [Eq. (3)] with different numbers of modes.

Here, $\hat{H}_{e,\mathbf{k}_\parallel}$ is the bare emitter Hamiltonian. The operators $a_{\mathbf{k}_\parallel,i}$ describe the effective lossy photonic modes of the metasurface, while $d^{(h)}_{\mathbf{k}_\parallel}$ describes the spin-wave excitations of the emitter array. Losses are included through Lindblad terms with rates $\kappa_{\mathbf{k}_\parallel,i}$, see SM [48]. The key point is that Eq. (2) is a cavity-QED Hamiltonian for an extended periodic platform: the coupling conserves Bloch momentum and hybridizes photonic and material excitations at the same $\mathbf{k}_\parallel$.

The parameters of Hamiltonian (2) are not phenomenological. They are obtained by requiring the effective model to reproduce the *ab initio* reciprocal-space spectral density, $\mathbf{J}_{\mathrm{mod}}(\mathbf{k}_\parallel,\omega) = \mathbf{J}(\mathbf{k}_\parallel,\omega)$, with

$$\mathbf{J}_{\mathrm{mod}}(\mathbf{k}_\parallel,\omega) = \frac{1}{\pi}\mathbf{g}_{\mathbf{k}_\parallel} \cdot \mathrm{Im}\left[\frac{1}{\tilde{\mathbf{H}}_{\mathbf{k}_\parallel} - \omega}\right] \cdot \mathbf{g}^\dagger_{\mathbf{k}_\parallel}, \tag{3}$$

and $\tilde{H}_{\mathbf{k}_\parallel,ij} = \omega_{\mathbf{k}_\parallel,ij} - \mathrm{i}\kappa_{\mathbf{k}_\parallel,i}\delta_{ij}/2$. This can be achieved by fitting the parameters of the few-mode model, namely the mode frequencies $\omega_{\mathbf{k}_\parallel,ii}$, the mode couplings $\omega_{\mathbf{k}_\parallel,ij}$, and the decay rates $\kappa_{\mathbf{k}_\parallel,i}$, as well as the light-matter coupling constants $g_{\mathbf{k}_\parallel,ih}$.

We apply this procedure to a representative SLR in the plasmonic array considered above; see Fig. 2. Even when the far-field spectrum suggests that SLRs are single-mode resonances, we find that a naive single-mode picture of SLRs can fail: the SLR line shape in the reciprocal-space spectral density is asymmetric, in contrast to the symmetric Lorentzian expected for a single mode [cf. Eq. (3)] [69]. Therefore, it cannot be reproduced by one Lorentzian mode. Physically, the asymmetry—and hence the multimode nature—can be attributed to the inherent asymmetry of the Rayleigh anomalies, which our few-mode model is able to fully capture, as seen in Fig. 2(d).

*Crystal polaritons in a quantum metasurface*—We now use the developed framework to demonstrate our main physical result: a commensurable emitter array and a dielectric or plasmonic metasurface can enter a collective strong-coupling regime in which the eigenmodes are hybrid light-matter Bloch excitations. All elements of this experimental setup can be achieved with state-of-the-art devices. We consider dipole moments of 10D realized, e.g., with quantum dots, defect emitters, or organic molecules, and use metasurface resonances with quality factors comparable to those found experimentally [42,48,70]. The main experimental challenge is to place the emitters in an array with fixed relative position to the nanoparticle. Promising platforms to do so are carbon-based color centers in hexagonal boron nitride films [23,71], atoms trapped by Casimir-Polder forces of the metasurface [72,73], or molecules placed via DNA origami [74,75].

For the plasmonic array considered above, we obtain the cavity QED parameters of the quantized surface lattice resonances from the fit of the few-mode model. We find that with a single emitter per unit cell that has a dipole moment of 10D, the setup is close but does not quite reach the strong-coupling regime. As discussed in the SM [48], the strong-coupling regime can be reached using slightly larger lattice constants $a > 615$ nm, however, requiring record high $Q$ factors [70] for the SLRs.

Much higher quality factors than those of SLRs in plasmonic systems can be achieved for bound states in the continuum (BICs) in dielectric nanoparticle arrays [42]. Therefore, we next consider a square array of dielectric (silicon) nanospheres and focus on a BIC originating from the magnetic dipole resonance of the spheres [76], see Fig. 3(a). We identify this BIC as an approximately Lorentzian resonance in the reciprocal-space spectral density, whose width narrows with decreasing in-plane wave vector; compare Figs. 3(c) and 3(d). As expected, the BIC resonance is much sharper than those of the plasmonic array discussed above, yielding much smaller decay rates, as we show below (see also the SM [48] for further details).

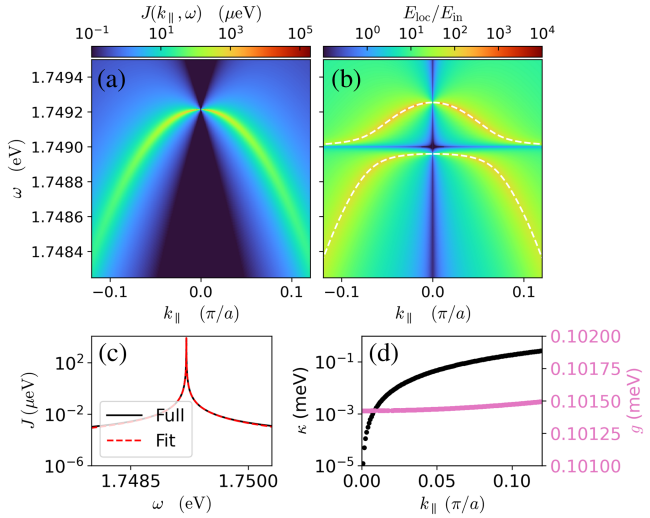


FIG. 3. Crystal-polariton formation with a bound state in the continuum. (a) Dispersion of the reciprocal-space spectral density $J$ for a square array of dielectric (silicon) nanospheres with radius $R = 100$ nm, refractive index $n = 3.5$, lattice constant $a = 400$ nm, $\mathbf{k}_\parallel = k_\parallel \mathbf{e}_y$, and the emitter array is positioned at $(0, 105\,\mathrm{nm}, 0)$ in the unit cell with frequency $\omega_E = 1.749$ eV, dipole moment $d = 10$ D, and orientation $\mathbf{n} = \mathbf{e}_x$. (b) Local field strength $E_{\rm loc}$ at the position of the emitter as a function of the frequency $\omega_L$ and in-plane momentum $\mathbf{k}_{\rm L} = k_{\rm L}\mathbf{e}_y$ of the plane-wave laser driving with amplitude $E_{\rm in}$ and polarization $\mathbf{e}_x$. The dispersion of the crystal polaritons is shown by the dashed lines. (c) Exemplary single-mode fit of $J$ at $k_\parallel = 6.4 \times 10^{-3}\pi/a$. (d) Coupling strength $g$ and decay rate $\kappa$ of the bound state in the continuum obtained from fitting a single-mode model to $J$ at different in-plane momenta.

We find that the BIC resonance in the reciprocal-space spectral density can be modeled by a single lossy mode for each value of the in-plane wave vector; see Fig. 3(c). We further obtain the decay rate and coupling strength of this mode to an emitter with a dipole moment of 10D and a frequency of $\omega_E = 1.749$ eV by a single-mode fit and show them as functions of in-plane momentum in Fig. 3(d). Although the decay rate vanishes when approaching the $\Gamma$ point at $\mathbf{k}_\parallel = \mathbf{0}$, leading to a divergent quality factor, we find that the coupling strength remains finite and essentially constant over the resolved wave-vector range. Clearly, we find $g > \kappa$, such that the system operates in the strong-coupling regime. To confirm this, we show the electric field at the position of the emitter under plane-wave driving with different in-plane momenta and frequencies in Fig. 3(b); see SM for details [48]. A clear anticrossing can be found that indicates the strong-coupling regime. The dispersion of these polariton modes can be obtained by diagonalizing the single excitation manifold of the few-mode Hamiltonian [white dashed line in Fig. 3(b)]. This offers a highly tunable strong-coupling platform, as many different crystal polaritons can be realized depending on the lattice geometry and the position of the emitter.

*Resonant quantum nonlinear optics with crystal polaritons*—The high $Q$ resonances of dielectric metasurfaces have already been shown to boost nonlinear light conversion in a series of experimental works relying on off-resonant light-matter interactions [42–45]. Because the matter component of crystal polaritons is composed of two-level excitations, these hybrid modes inherit a strong quantum nonlinearity. As a first application of crystal polaritons, we therefore show how driving them with a laser can lead to resonant nonlinear light generation with an increase in the nonlinear light conversion by many orders of magnitude compared to conventional platforms based on bulk nonlinearities [42–45].

In the low-excitation regime, we can approximate the two-level emitters by harmonic oscillators with annihilation operators $\hat{b}_{\mathbf{k}_\parallel}$. As a result, $\mathbf{k}_\parallel$ is conserved on the single particle level. We introduce the nonlinearity of the two-level emitters via the resummation of the Holstein-Primakoff expansion [77,78] of $\hat{\sigma}_{\mathbf{k}_\parallel}$ in terms of $\hat{b}_{\mathbf{k}_\parallel}$, resulting in a polariton-polariton scattering term in the Hamiltonian [48]. A strong nonlinear response with just one excitation in the system arises when this term induces a frequency shift of the two-polariton state that is larger than its linewidth [79–81]. For our system, we find that this is satisfied for polariton densities as low as one polariton per 10.7 $\mu$m$^2$ ($= 67$ unit cells) [48], and should also be compared to the free-space wavelength of 0.71 $\mu$m of the laser driving. This demonstrates the potential of our setup for quantum optical applications, which we will explicitly demonstrate using the example of the efficient generation of directionally emitted entangled photon pairs [see Fig. 4(a)].

To this end, we introduce laser driving with fixed frequency $\omega_L$ and in-plane momentum $\mathbf{k}_L$, see Fig. 4(a), accounting for light scattering at the metasurface self-consistently following Refs. [82,83], as outlined in the SM [48]. In the low-excitation regime and in the steady state the laser driving coherently displaces the modes and the emitters with momentum $\mathbf{k}_L$ by $\mathscr{a}_{\mathbf{k}_L,i}$ and $\mathscr{b}_{\mathbf{k}_L}$, respectively, while all emitter and photon states with $\mathbf{k}_\parallel \neq \mathbf{k}_L$ remain in the ground state. Assuming that the nonlinearity is weak, we find that the lowest-order correction affecting modes with $\mathbf{k}_\parallel \neq \mathbf{k}_{\rm L}$ is given by a squeezing and a beam-splitter contribution [48]. The beam-splitter contribution leads to a negligible shift of the mode and emitter frequencies, while the squeezing Hamiltonian leads to the generation of entangled excitations and reads $\hat{H}_{\mathrm{sq},\mathbf{k}_\parallel} = \sum_i g^*_{\mathbf{k}_\parallel,i}\mathscr{b}^2_{\mathbf{k}_{\rm L}}\hat{a}^\dagger_{\mathbf{k}_\parallel,i}\hat{b}^\dagger_{\bar{\mathbf{k}}_\parallel} + E_{\rm loc}\mathscr{b}_{\mathbf{k}_{\rm L}}\hat{b}^\dagger_{\mathbf{k}_\parallel}\hat{b}^\dagger_{\bar{\mathbf{k}}_\parallel} + (\mathbf{k}_\parallel \leftrightarrow \bar{\mathbf{k}}_\parallel) + \mathrm{H.c.}$, where $(\mathbf{k}_\parallel \leftrightarrow \bar{\mathbf{k}}_\parallel)$ denotes adding the preceding terms subject to the replacement $\mathbf{k}_\parallel \leftrightarrow \bar{\mathbf{k}}_\parallel$ with $\bar{\mathbf{k}}_\parallel \equiv 2\mathbf{k}_{\rm L} - \mathbf{k}_\parallel$. Allowing for up to two excitations in the system, we can numerically identify the steady-state two-photon emission rate at a fixed wave vector $\mathbf{k}_\parallel$ defined

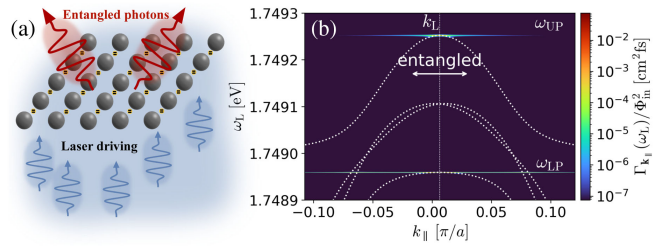


FIG. 4. Resonant quantum light generation from crystal-polariton nonlinearities. (a) Schematic of the proposed setup. (b) Two-photon emission rate density $\Gamma_{\mathbf{k}_\parallel}$ normalized by the incoming flux density $\Phi_{in}^2$ ($\Gamma_{\mathbf{k}_\parallel} \propto \Phi_{in}^2$ in the perturbative regime) for $k_L = 6.4 \times 10^{-3}\pi/a$ (vertical dotted line) and $V_d/V_B = 1.6 \times 10^{-5}$ as a function of laser frequency $\omega_L$ and in-plane momentum $\mathbf{k}_\parallel = k_\parallel \mathbf{e}_y$ of one of the emitted photons (in-plane momentum of the other emitted photon is fixed to $2k_L - k_\parallel$ such that the plot is symmetric around $k_L$). Enhanced two-photon emission occurs when the laser frequency is in resonance with the upper or lower crystal polaritons at the laser momentum $\omega_{UP/LP}$ and the resonance condition $\omega(\mathbf{k}_\parallel) + \omega(\bar{\mathbf{k}}_\parallel) = 2\omega_L$, shown by white dashed lines, is satisfied.

by $\gamma_{\mathbf{k}_\parallel} = \sum_{i,j}(\kappa_{\mathbf{k}_\parallel,i} + \kappa_{\bar{\mathbf{k}}_\parallel,j})\langle \hat{a}^\dagger_{\mathbf{k}_\parallel,i}\hat{a}^\dagger_{\bar{\mathbf{k}}_\parallel,j}\hat{a}_{\mathbf{k}_\parallel,i}\hat{a}_{\bar{\mathbf{k}}_\parallel,j}\rangle_{ss}$. Here, $\langle \ldots \rangle_{ss}$ is the steady-state expectation value. The two-photon emission rate density per unit area into a certain range of wave vectors $\mathbf{k}_\parallel \in V_d$ is defined by $\Gamma_{V_d} = 1/(4\pi^2)\int_{V_d} \mathrm{d}^2 k_\parallel \gamma_{\mathbf{k}_\parallel}$ and can be approximated by $\Gamma_{\mathbf{k}_\parallel} = V_d/(4\pi^2)\gamma_{\mathbf{k}_\parallel}$ for small $V_d$. Note that since the squeezing Hamiltonian $\hat{H}_{sq,\mathbf{k}_\parallel}$ always generates pairs of excitations at $\mathbf{k}_\parallel$ and $\bar{\mathbf{k}}_\parallel$, the emitted photons are strongly entangled and we only have to integrate over a single wave vector $\mathbf{k}_\parallel$, while the wave vector of the other emitted photon is fixed by momentum conservation to $2\mathbf{k}_L - \mathbf{k}_\parallel$.

In Fig. 4(b), we plot $\Gamma_{\mathbf{k}_\parallel}$ for $k_L = 6.4 \times 10^{-3}\pi/a$ as a function of the laser driving frequency $\omega_L$ and the in-plane momentum of one of the emitted photons $\mathbf{k}_\parallel$. The maxima in the two-photon emission rates can be understood as a result of two resonant conditions: (i) the laser driving has to be resonant with one of the polaritonic modes $\omega_{UP}$ and $\omega_{LP}$ at $\mathbf{k}_L$ [the maxima in Fig. 4(b) are clearly centered around $\omega_{UP}$ and $\omega_{LP}$]; (ii) and momentum (phase matching) and energy must be conserved, i.e., there must be polaritonic modes with frequencies $\omega(\mathbf{k}_\parallel)$ and $\omega(\bar{\mathbf{k}}_\parallel)$ satisfying $\omega(\mathbf{k}_\parallel)+\omega(\bar{\mathbf{k}}_\parallel)=2\omega_L$. These conditions are plotted by the white dashed lines in Fig. 4(b). As a result of both resonant conditions, we see maxima in the two-photon emission rate when the dashed lines cross $\omega_{LP}$ or $\omega_{UP}$ in Fig. 4(b). We find that the normalized two-photon emission rate $\Gamma_{\mathbf{k}_\parallel}/\Phi_{in}^2$ emitted into a narrow fraction $V_d/V_B = 1.6 \times 10^{-5}$ of the Brillouin zone $V_B = (2\pi/a)^2$ can reach values up to $10^{-2}$ cm$^2$ fs. This means that for an incoming laser power density of, e.g., just $P = 10\ \mu\mathrm{W/cm^2}$ the conversion efficiency into that narrow range of wave vectors is $\Gamma_{\mathbf{k}_\parallel}/\Phi_{in} = 3.6 \times 10^{-4}$ and for $P > 28\ \mathrm{mW/cm^2}$ the system would already be far in the nonperturbative regime (perturbative conversion efficiency $> 1$). Nonlinear metasurfaces with dielectric nanoparticles based on off-resonant bulk nonlinearities [42–45] have experimentally reached conversion efficiencies of $10^{-6}$ at laser powers of 60 MW/cm$^2$, which makes our platform theoretically more efficient by 14 orders of magnitude within the narrow resonant frequency window. While practical limitations like fabrication disorder or finite size effects will moderate this theoretical value, it still illustrates the fundamental enhancement.

*Conclusion and outlook*—In summary, we have shown that metasurfaces can be promoted from classical wave-shaping elements to a tunable cavity-QED platform for periodic quantum matter. Treating photonic Bloch resonances and emitter-array spin waves on equal footing, we have shown that they can hybridize into crystal polaritons with a nonlinear optical response that can be used for efficient quantum light generation. The complete setup can be seen as a polaritonic quantum metasurface with many different design possibilities. Here, we have focused on wavelength-sized arrays, but subwavelength arrays are also expected to offer great potential for quantum optics [28–35,37,38,40]. Moreover, chiral electromagnetic modes, whose design in typical cavity QED platforms is challenging and which are of particular interest in chiral sensing and nonreciprocal quantum devices, as well as topologically nontrivial states of finite-sized metasurfaces, could be harnessed in the future by the proposed polaritonic quantum metasurface.

*Acknowledgments*—We thank Jaime Abad-Arredondo and Alberto Miguel-Torcal for fruitful discussions. We acknowledge financial support by the Spanish Ministerio de Ciencia y Universidades—Agencia Estatal de Investigación through Grants No. PID2021-125894NB-I00, No. PID2024-161142NB-I00, No. EUR2023-143478, and No. CEX2023-001316-M through the María de Maeztu program for Units of Excellence in R&D, and from the European Union's Horizon Europe research and innovation programme under Grant Agreements No. 101070700 (MIRAQLS) and No. 101098813 (SCOLED). The work was further supported by the ETH Quantum Center Research Fellowship and the Dr. Alfred and Flora Spälti Fonds.

*Data availability*—The data that support the findings of this article are not publicly available. The data are available from the authors upon reasonable request.

[1] S. Haroche and J.-M. Raimond, *Exploring the Quantum: Atoms, Cavities, and Photons* (Oxford University Press, Oxford, 2006).
[2] C. L. Degen, F. Reinhard, and P. Cappellaro, Rev. Mod. Phys. **89**, 035002 (2017).
[3] H. J. Kimble, Nature (London) **453**, 1023 (2008).

[4] D. E. Chang, J. S. Douglas, A. González-Tudela, C.-L. Hung, and H. J. Kimble, Rev. Mod. Phys. **90**, 031002 (2018).

[5] J. Fregoni, F. J. Garcia-Vidal, and J. Feist, ACS Photonics **9**, 1096 (2022).

[6] A. González-Tudela, A. Reiserer, J. J. García-Ripoll, and F. J. García-Vidal, Nat. Rev. Phys. **6**, 166 (2024).

[7] S. Zou, N. Janel, and G. C. Schatz, J. Chem. Phys. **120**, 10871 (2004).

[8] S. Mukherjee, A. Spracklen, D. Choudhury, N. Goldman, P. Öhberg, E. Andersson, and R. R. Thomson, Phys. Rev. Lett. **114**, 245504 (2015).

[9] L. Lu, C. Fang, L. Fu, S. G. Johnson, J. D. Joannopoulos, and M. Soljačić, Nat. Phys. **12**, 337 (2016).

[10] X. Ni, S. Yves, A. Krasnok, and A. Alu, Chem. Rev. **123**, 7585 (2023).

[11] B. Bahari, A. Ndao, F. Vallini, A. El Amili, Y. Fainman, and B. Kanté, Science **358**, 636 (2017).

[12] M. A. Bandres, S. Wittek, G. Harari, M. Parto, J. Ren, M. Segev, D. N. Christodoulides, and M. Khajavikhan, Science **359**, eaar4005 (2018).

[13] C. Han, M. Kang, and H. Jeon, ACS Photonics **7**, 2027 (2020).

[14] S. Fan and J. D. Joannopoulos, Phys. Rev. B **65**, 235112 (2002).

[15] Y. Plotnik, O. Peleg, F. Dreisow, M. Heinrich, S. Nolte, A. Szameit, and M. Segev, Phys. Rev. Lett. **107**, 183901 (2011).

[16] C. W. Hsu, B. Zhen, J. Lee, S.-L. Chua, S. G. Johnson, J. D. Joannopoulos, and M. Soljačić, Nature (London) **499**, 188 (2013).

[17] C. W. Hsu, B. Zhen, A. D. Stone, J. D. Joannopoulos, and M. Soljačić, Nat. Rev. Mater. **1**, 16048 (2016).

[18] V. M. Shalaev, Nat. Photonics **1**, 41 (2007).

[19] J. D. Joannopoulos, P. R. Villeneuve, and S. Fan, Solid State Commun. **102**, 165 (1997).

[20] T. Santiago-Cruz, S. D. Gennaro, O. Mitrofanov, S. Addamane, J. Reno, I. Brener, and M. V. Chekhova, Science **377**, 991 (2022).

[21] A. S. Solntsev, G. S. Agarwal, and Y. S. Kivshar, Nat. Photonics **15**, 327 (2021).

[22] A. I. Väkeväinen, R. J. Moerland, H. T. Rekola, A.-P. Eskelinen, J.-P. Martikainen, D.-H. Kim, and P. Törmä, Nano Lett. **14**, 1721 (2014).

[23] T. T. H. Do, M. Nonahal, C. Li, V. Valuckas, H. H. Tan, A. I. Kuznetsov, H. S. Nguyen, I. Aharonovich, and S. T. Ha, Nat. Commun. **15**, 2281 (2024).

[24] M. Ramezani, A. Halpin, A. I. Fernández-Domínguez, J. Feist, S. R.-K. Rodriguez, F. J. Garcia-Vidal, and J. Gómez Rivas, Optica **4**, 31 (2016).

[25] A. I. Väkeväinen, A. J. Moilanen, M. Nečada, T. K. Hakala, K. S. Daskalakis, and P. Törmä, Nat. Commun. **11**, 3139 (2020).

[26] T. K. Hakala, A. J. Moilanen, A. I. Väkeväinen, R. Guo, J.-P. Martikainen, K. S. Daskalakis, H. T. Rekola, A. Julku, and P. Törmä, Nat. Phys. **14**, 739 (2018).

[27] F. Verdelli, Y.-C. Wei, K. Joseph, M. S. Abdelkhalik, M. Goudarzi, S. H. Askes, A. Baldi, E. Meijer, and J. Gomez Rivas, Angew. Chem., Int. Ed. Engl. **63**, e202409528 (2024).

[28] E. Shahmoon, D. S. Wild, M. D. Lukin, and S. F. Yelin, Phys. Rev. Lett. **118**, 113601 (2017).

[29] J. Perczel, J. Borregaard, D. E. Chang, H. Pichler, S. F. Yelin, P. Zoller, and M. D. Lukin, Phys. Rev. A **96**, 063801 (2017).

[30] J. Rui, D. Wei, A. Rubio-Abadal, S. Hollerith, J. Zeiher, D. M. Stamper-Kurn, C. Gross, and I. Bloch, Nature (London) **583**, 369 (2020).

[31] R. J. Bettles, M. D. Lee, S. A. Gardiner, and J. Ruostekoski, Commun. Phys. **3**, 141 (2020).

[32] M. Moreno-Cardoner, D. Goncalves, and D. E. Chang, Phys. Rev. Lett. **127**, 263602 (2021).

[33] L. Zhang, V. Walther, K. Mølmer, and T. Pohl, Quantum **6**, 674 (2022).

[34] S. P. Pedersen, L. Zhang, and T. Pohl, Phys. Rev. Res. **5**, L012047 (2023).

[35] S. P. Pedersen, G. M. Bruun, and T. Pohl, Phys. Rev. Res. **6**, 043264 (2024).

[36] B. Durá-Azorín, A. I. Fernández-Domínguez, and A. Manjavacas, arXiv:2510.19992.

[37] A. Asenjo-Garcia, M. Moreno-Cardoner, A. Albrecht, H. J. Kimble, and D. E. Chang, Phys. Rev. X **7**, 031024 (2017).

[38] D. Bluvstein, S. J. Evered, A. A. Geim, S. H. Li, H. Zhou, T. Manovitz, S. Ebadi, M. Cain, M. Kalinowski, D. Hangleiter *et al.*, Nature (London) **626**, 58 (2024).

[39] M. Morgado and S. Whitlock, AVS Quantum Sci. **3**, 023501 (2021).

[40] M. Reitz, C. Sommer, and C. Genes, PRX Quantum **3**, 010201 (2022).

[41] M. Reitz, S. v. d. Wildenberg, A. Koner, G. C. Schatz, and J. Yuen-Zhou, Nanophotonics **15**, e70008 (2026).

[42] Z. Liu, Y. Xu, Y. Lin, J. Xiang, T. Feng, Q. Cao, J. Li, S. Lan, and J. Liu, Phys. Rev. Lett. **123**, 253901 (2019).

[43] K. Koshelev, Y. Tang, K. Li, D.-Y. Choi, G. Li, and Y. Kivshar, ACS Photonics **6**, 1639 (2019).

[44] Y. Yang, W. Wang, A. Boulesbaa, I. I. Kravchenko, D. P. Briggs, A. Puretzky, D. Geohegan, and J. Valentine, Nano Lett. **15**, 7388 (2015).

[45] G. Grinblat, ACS Photonics **8**, 3406 (2021).

[46] H.-P. Breuer and F. Petruccione, *The Theory of Open Quantum Systems* ( Oxford University Press, Oxford, 2002).

[47] P. Menczel, K. Funo, M. Cirio, N. Lambert, and F. Nori, Phys. Rev. Res. **6**, 033237 (2024).

[48] See Supplemental Material at http://link.aps.org/supplemental/10.1103/71nx-b83j for detailed derivations of the results reported in the main text, which includes Refs. [49–56].

[49] S. Y. Buhmann and D.-G. Welsch, Phys. Rev. A **77**, 012110 (2008).

[50] S. Y. Buhmann, *Dispersion Forces I* (Springer, Berlin, 2012).

[51] D. Beutel, I. Fernandez-Corbaton, and C. Rockstuhl, Comput. Phys. Commun. **297**, 109076 (2024).

[52] A. Ben-Asher, A. I. Fernández-Domínguez, and J. Feist, Phys. Rev. Lett. **130**, 243601 (2023).

[53] M. O. Scully and M. S. Zubairy, *Quantum Optics* (Cambridge University Press, Cambridge, England, 1997).

[54] F. J. García de Abajo, Rev. Mod. Phys. **79**, 1267 (2007).

[55] Y. Liang, D. P. Tsai, and Y. Kivshar, Phys. Rev. Lett. **133**, 053801 (2024).

[56] P. Törmä and W. L. Barnes, Rep. Prog. Phys. **78**, 013901 (2014).
[57] R. E. Jorgenson and R. Mittra, IEEE Trans. Antennas Propag. **38**, 633 (2002).
[58] C. M. Linton, SIAM Rev. **52**, 630 (2010).
[59] S. Scheel and S. Buhmann, Acta Phys. Slovaca **58**, 675 (2008).
[60] A. Delga, J. Feist, J. Bravo-Abad, and F. J. Garcia-Vidal, Phys. Rev. Lett. **112**, 253601 (2014).
[61] E. D. Palik, *Handbook of Optical Constants of Solids* (Academic Press, New York, 1998), Vol. 3.
[62] C. Cherqui, M. R. Bourgeois, D. Wang, and G. C. Schatz, Acc. Chem. Res. **52**, 2548 (2019).
[63] D. Tamascelli, A. Smirne, S. F. Huelga, and M. B. Plenio, Phys. Rev. Lett. **120**, 030402 (2018).
[64] D. Lentrodt and J. Evers, Phys. Rev. X **10**, 011008 (2020).
[65] I. Medina, F. J. García-Vidal, A. I. Fernández-Domínguez, and J. Feist, Phys. Rev. Lett. **126**, 093601 (2021).
[66] M. Sánchez-Barquilla, F. J. García-Vidal, A. I. Fernández-Domínguez, and J. Feist, Nanophotonics **11**, 4363 (2022).
[67] C. J. Sánchez Martínez, J. Feist, and F. J. García-Vidal, Nanophotonics **13**, 2669 (2024).
[68] M. Lednev, D. Fernández de la Pradilla, F. Lindel, E. Moreno, F. J. García-Vidal, and J. Feist, PRX Quantum **6**, 020361 (2025).
[69] D. Lentrodt, O. Diekmann, C. H. Keitel, S. Rotter, and J. Evers, Phys. Rev. Lett. **130**, 263602 (2023).
[70] M. S. Bin-Alam, O. Reshef, Y. Mamchur, M. Z. Alam, G. Carlow, J. Upham, B. T. Sullivan, J.-M. Ménard, M. J. Huttunen, R. W. Boyd *et al.*, Nat. Commun. **12**, 974 (2021).
[71] T. T. Tran, K. Bray, M. J. Ford, M. Toth, and I. Aharonovich, Nat. Nanotechnol. **11**, 37 (2016).
[72] M. Gullans, T. G. Tiecke, D. E. Chang, J. Feist, J. D. Thompson, J. I. Cirac, P. Zoller, and M. D. Lukin, Phys. Rev. Lett. **109**, 235309 (2012).
[73] A. González-Tudela, C.-L. Hung, D. E. Chang, J. I. Cirac, and H. Kimble, Nat. Photonics **9**, 320 (2015).
[74] R. J. Kershner, L. D. Bozano, C. M. Micheel, A. M. Hung, A. R. Fornof, J. N. Cha, C. T. Rettner, M. Bersani, J. Frommer, P. W. Rothemund *et al.*, Nat. Nanotechnol. **4**, 557 (2009).
[75] A. Kuzyk, R. Jungmann, G. P. Acuna, and N. Liu, ACS Photonics **5**, 1151 (2018).
[76] D. R. Abujetas and J. A. Sánchez-Gil, Nanomater. Nanotechnol. **11**, 998 (2021).
[77] T. Holstein and H. Primakoff, Phys. Rev. **58**, 1098 (1940).
[78] M. Vogl, P. Laurell, H. Zhang, S. Okamoto, and G. A. Fiete, Phys. Rev. Res. **2**, 043243 (2020).
[79] D. E. Chang, V. Vuletić, and M. D. Lukin, Nat. Photonics **8**, 685 (2014).
[80] A. Delteil, T. Fink, A. Schade, S. Höfling, C. Schneider, and A. İmamoğlu, Nat. Mater. **18**, 219 (2019).
[81] G. Muñoz-Matutano, A. Wood, M. Johnsson, X. Vidal, B. Q. Baragiola, A. Reinhard, A. Lemaître, J. Bloch, A. Amo, G. Nogues *et al.*, Nat. Mater. **18**, 213 (2019).
[82] J. Feist, A. I. Fernández-Domínguez, and F. J. García-Vidal, Nanophotonics **10**, 477 (2020).
[83] F. Lindel, R. Bennett, and S. Y. Buhmann, Phys. Rev. A **103**, 033705 (2021).